Optical and microstructural properties of MgF_2 UV coatings grown by ion beam sputtering process

E. Quesnel[a] and L. Dumas
LETI/CEA-G-DOPT, 17 rue des Martyrs, 38054 Grenoble cedex 9, France

D. Jacob and F. Peiró
EME, Ingeniería y Materiales Electrónicos, Departamento de Electrónica, Universidad de Barcelona, Marti i Franquès, 1, E-08028 Barcelona, España

(Received 22 December 1999; accepted 10 July 2000)

The optical, mechanical, and microstructural properties of MgF_2 single layers grown by ion beam sputtering have been investigated by spectrophotometric measurements, film stress characterization, x-ray photoelectron spectroscopy (XPS), x-ray diffraction, and transmission electron microscopy. The deposition conditions, using fluorine reactive gas or not, have been found to greatly influence the optical absorption and the stress of the films as well as their microstructure. The layers grown with fluorine compensation exhibit a regular columnar microstructure and an UV-optical absorption which can be very low, either as deposited or after thermal annealings at very low temperatures. On the contrary, layers grown without fluorine compensation exhibit a less regular microstructure and a high ultraviolet absorption which is particularly hard to cure. On the basis of calculations, it is shown that F centers are responsible for this absorption, whereas all the films were found to be stoichiometric, in the limit of the XPS sensitivity. On the basis of external data taken from literature, our experimental curves are analyzed, so we propose possible diffusion mechanisms which could explain the behaviors of the coatings.
[S0734-2101(00)00406-1]

I. INTRODUCTION

Fluorides such as MgF_2 are typical materials to make optical coatings for laser applications in the ultraviolet (UV) spectral range.[1] The coatings, conventionally grown by evaporation, generally exhibit relatively low optical losses and a high packing density, provided that the deposition is performed at high temperature, namely in the range of 250–300 °C. Such deposition conditions lead, however, to rougher films, which can induce optical scattering.

In modern applications, such as semiconductor lithography, the trend to lower wavelengths requires improving the quality of the coatings towards smoother films, in particular. Thus, for many years, various attempts of improvement have been achieved using, for instance, ion assisted deposition techniques to get denser films at low deposition temperature.[2,3] Nevertheless, this ion-induced densification was found to create a strong optical absorption in the films, which makes them properly unusable for deep ultraviolet (DUV) applications. As a more innovative growth technique, the ion beam sputtering (IBS) of MgF_2 target offers good perspectives to enhance the layer quality. The major advantage of the technique is to produce, at ambient temperature, coatings with higher packing density and thus reduced optical scattering.[4] Up to recently, the major obstacle to the use of sputtering techniques for the deposition of MgF_2 coatings has resulted from the high optical absorption of the films. Whatever the sputtering techniques, either cathodic sputtering[5] or IBS,[6,7] the extinction coefficient (k) of the MgF_2 films at a wavelength $\lambda = 400$ nm and lower, never dropped below 10^{-2}. A common explanation for this phenomenon generally is the nonideal stoichiometry of the films attributed to preferential sputtering of lighter atoms by energetic species impinging onto the growing film. Nevertheless, more recently and thanks to a new reactive deposition process, very low absorbing IBS MgF_2 films have been successfully produced with k coefficients in the range of 10^{-6}.[8]

In this context, the present study deals with the characterization of IBS-grown MgF_2 coatings. It mainly aims at bringing new elements to improve the understanding of the origin of optical absorption in sputtered MgF_2 coatings. Therefore, the deposition conditions of IBS MgF_2 films have been intentionally varied widely. We present here the most significant results regarding the microstructural, mechanical, chemical, as well as optical characteristics of the films.

II. EXPERIMENTAL PROCEDURE

A. Sample preparation

For this study, different samples were produced in various deposition conditions. For each run, three different substrates were used: UV-grade silica samples, Si(111) 2 in. wafers, and specific bar-shaped Si(111) substrates [(50×5) mm^2 and 1 mm thick]. The silica samples were dedicated to optical characterizations. The different silicon substrates assigned for the other characterizations were first covered with a thin alumina sputtered film to warrant a good adhesion of the MgF_2 layers. The film deposition was performed in a load-locked IBS chamber equipped with two cryo pumps leading to a base pressure of 4×10^{-8} mbar. During deposition, the

[a]Electronic mail: quesnel@chartreuse.cea.fr

TABLE I. Typical characteristics of deposited samples.

Sample	Process	P_{F_2}/s[a] (10^{-6} mbar Å^{-1} s)	Thickness (nm)	n at 351 nm	k at 351 nm	Stress σ (MPa)	Grain size (nm)
R_0	Nonreactive	0	475	1.41	3.3×10^{-2}	+79	40
R_1	Reactive	5.7	320	1.387	1×10^{-2}	−117	30
R_2	Reactive	6.3	290	1.390	4.4×10^{-3}	−537	30
R_3	Reactive	6.6	217	1.394	1.4×10^{-3}	−636	25
R_4	Reactive	7.6	203	1.391	8×10^{-6}	−910	25

[a]See definition in text.

substrate temperature remained lower than 60 °C and the operating pressure was fixed at 1×10^{-4} mbar. The target-to-substrate distance is equal to 50 cm.

The first deposition run (denoted R_0) was performed by simply sputtering a hot-pressed MgF_2 target with xenon ions accelerated at an energy of 900 eV. As we will see, these operating conditions led to the production of slightly brownish films which exhibit rather high optical losses. Such a phenomenon has been already observed in a previous study[4] we made on other fluoride films, namely IBS YF_3 films, and, on the basis of composition measurements, it was clearly attributed to fluorine deficiency in the films. That is why, for the present work, other MgF_2 samples were prepared using reactive deposition conditions which were gradually improved (runs R_1 to R_4). We based this improvement on two main ideas which consist of the necessity of: (i) bringing additional fluorine to the sputtered target and to the growing film, (ii) reducing the ion bombardment of the growing MgF_2 films. The reduction of ion bombardment is obtained by using xenon as sputtering gas instead of argon, limiting that way the flux of reflected ions by the target. The supply of additional fluorine was initially achieved by introducing CF_4 gas in the deposition chamber. For the present purpose and since DUV applications are concerned, diluted fluorine is now preferred in order to limit the carbon contamination. The carbon is indeed known to promote strong DUV optical losses.[9] The diluted fluorine we used is a mixture of 10% F_2 in argon. During deposition, the flow rate of diluted fluorine was equal to 5 sccm, which corresponded to a partial pressure of fluorine P_{F2} of around 2×10^{-6} mbar. From run R_1 to R_4 the operating conditions were thus varied by decreasing the Xe^+ ion flux arriving at the MgF_2 target relative to the F_2 concentration in the chamber. As a result, the film deposition rate (s) decreases from 0.35 to 0.25 Å/s. If we assume that the fluorination of the deposited films occurs mainly at the substrate surface, its efficiency would then depend on the flux ratio between the additional fluorine (introduced in the chamber) which diffuses towards the substrate (v_{F2}) and the sputtered Mg and F atoms coming from the target ($v_{\mathrm{Mg}}+2v_F$). Since v_{F2} depends on the fluorine partial pressure P_{F2}, and ($v_{\mathrm{Mg}}+2v_F$) depends on the deposition rate s, the fluorination efficiency is directly related to the P_{F2}/s ratio. This ratio is not dependent on chamber geometry or pumping system and constitutes a relevant process parameter, usable by an experimenter, to define each deposition run (see Table I).

B. Optical characterizations

In order to evaluate the efficiency of the reactive deposition conditions, a systematic optical characterization was performed on each sample deposited on silica. The reflection (R) and transmission (T) spectra were recorded between 200 and 800 nm using a λ9 Perkin-Elmer spectrophotometer. This spectrophotometer is equipped with a homemade accessory which enables us to measure the transmission and reflection of the sample at exactly the same irradiated area. As a result, the absolute measurement accuracy is less than ±0.3%. From these measurements, the thickness and optical constants (n, k) of the films were calculated, in particular their extinction coefficient dispersion curves [$k(\lambda)$] which are related to the optical losses in the films. For this purpose, we used a nonlinear regression technique and assumed a Cauchy law for the refractive index dispersion [$n(\lambda)$]. The extinction coefficient dispersion curve was calculated by fitting theory to the measured normalized losses (NL) of the coating given by the following relation: $\mathrm{NL}(\lambda)=[(1-R(\lambda)-T(\lambda)]/T(\lambda)$.

C. Physical characterizations

The physical film characterizations comprise mechanical stress measurements, crystallographic analyses, and transmission electron microscopy (TEM). The film stress measurements, performed just after deposition, were done on bar-shaped silicon substrates using an interferometric technique. The residual stress (σ) was deduced from the change of curvature radius of the samples using the Stoney equation

$$\sigma=[E_s/(6(1-v_s)]\cdot[e_s^2/e_f]\cdot[r_2^{-1}-r_1^{-1}],$$

where $E_s/(1-v_s)$ is the biaxial modulus (229 GPa for the Si substrate), e_s and e_f are the substrate, and MgF_2 film thicknesses, respectively, and r_1 and r_2 are the radii of curvature of the substrate before and after MgF_2 deposition, respectively.

The crystalline structure was determined by x-ray diffraction (XRD) using grazing incidence of a Cu $K\alpha$ line in a Siemens D500 instrument. Concerning TEM, plane-view specimens were prepared by conventional mechanical grinding and dimpling up to 30 μm followed by a final Ar^+ ion bombardment on the substrate side at low angle of incidence (6°) and at 3 kV in a Gatan precision ion polishing system. For cross-section observations, samples were prepared using the same procedure on previously cleaved and face to face

glued samples. The observations were achieved on Hitachi H-800 NA and Philips CM30 electron microscopes working at 200 and 300 kV, respectively. Due to the instability of fluoride layers under electron beam illumination, low dose observation conditions were used.

D. Composition analyses

The composition determination and the detection of contamination levels were carried out by x-ray photoelectron spectroscopy (XPS) with a Perkin-Elmer Phi 5500 instrument using monochromatic Al $K\alpha$ line. In order to test the composition homogeneity across the layer, depth profile spectra were obtained using an Ar^+ bombardment at low energy (3 keV). High-resolution scans over the F $1s$, Mg $2s$, Si $2p$, C $1s$, O $1s$, and Al $2p$ peaks were taken after each bombardment period with a step size of 0.25 eV.

III. RESULTS

The main characteristics of the different samples are summarized in Table I. As mentioned in Sec. II A, the different process conditions are described by the P_{F2}/s experimental parameter. This parameter increases from run R_0 to R_4, which corresponds to an improvement of the fluorination conditions. The extinction coefficients of the films measured at $\lambda = 351$ nm (k at 351 nm values) are a good indication of their optical quality level. At the same time, whatever the deposition conditions, the films exhibit a low refractive index which remains very close to the one of bulk MgF_2. As expected, from R_0 to R_4, there is a drastic decrease of k. It is worth noting that for the R_4 sample, which is a particularly low absorbent (lowest k value), k was measured using a photothermal deflection technique, which is far more sensitive than spectrophotometry. As shown in Table I, the modification of the optical properties is accompanied by a change in the mechanical stresses. For nonreactive deposition conditions, the stress is slightly tensile, whereas from R_1 to R_4, for reactive conditions, the stress becomes more and more compressive. The meaning of these stress values must be carefully analyzed. We know, indeed, that different processes contribute to the overall residual stress. The first component σ_{th} of the stress comes from the thermal mismatch between substrate and film. If we assume that, whatever the sample, the deposition temperature is constant during the whole deposition run ($T_d \sim 60\,^\circ\text{C}$), we have

$$\sigma_{\text{th}} = [E_f/1-\upsilon_f]\cdot[\alpha_{\text{Si}} - \alpha_{\text{MgF}_2}]\cdot[20 - T_d],$$

where E_f and υ_f are Young and Poisson moduli of the MgF_2 film, respectively, α_{Si} and α_{MgF_2} are the expansion coefficients of substrate and MgF_2 film, respectively. Taking $E_f = 137$ GPa, $\upsilon_f = 0.3$, $\alpha_{\text{Si}} = 2.5\times10^{-6}\,\text{K}^{-1}$, and $\alpha_{\text{MgF}_2} = 13.7\times10^{-6}\,\text{K}^{-1}$ leads to an estimation of the thermal stress component of $+87$ MPa. The other stress components are the intrinsic component (σ_i), related to the deposition process itself, and the extrinsic stress component (σ_e) due to the interaction of the film with its environment (in particular water vapor). In the case of our sputtered films, the films are dense ($d = 3.14\,\text{g cm}^3$) and free of water so that σ_e can be neglected ($\sigma_e \approx 0$). This assumption is backed up by the fact that after 40 days of aging in room air, the stress level remains perfectly unchanged. So we have

$$\sigma = \sigma_i + \sigma_{\text{th}}.$$

Using this expression of the residual stress for the analysis of data from Table I leads to the conclusion that, in the nonreactive deposition conditions, the process does not induce any intrinsic stress except some low tensile thermal ones. On the contrary, for the reactive fluorine conditions, from R_1 to R_4 samples, the thermal contribution decreases in comparison with the compressive intrinsic stress component which becomes more and more dominant.

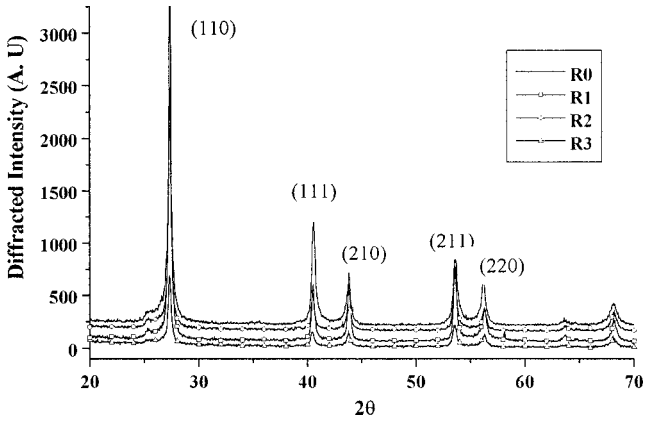

FIG. 1. Grazing incidence XRD spectra of some samples.

We must now examine the crystallographic structure of the films. The grazing incidence XRD spectra achieved on different samples are presented in Fig. 1. These spectra are characteristic of well-defined polycrystalline structures. As deduced from the positions of the peaks, the crystallographic nature of the samples corresponds to the tetragonal $P4_2/mnm$ phase of MgF_2. Furthermore, the comparison of the diffraction peak intensities with theory values (structure factor), indicates first, that a slight $\langle 110 \rangle$ texture exists in the samples and second, that the less textured sample is sample R_0.

In order to complete the structure analyses of the films, TEM observations have been performed. In Fig. 2 typical TEM plane-view observations made on four samples and their corresponding selected area diffraction (SAD) patterns are reproduced. The polycrystalline structure of the samples is clearly seen in these pictures. It is worth noting that on the pattern of Fig. 2(a), the intense and isolated spots are due to the Si substrate. Statistical measurements of the medium grain size give the results reported in Table I. From sample R_4 to sample R_0, the grain size increases slightly from 25 to 40 nm as the coating thickness does. On sample R_1, due to the higher thickness of the layer, the $\langle 110 \rangle$ texture can be locally observed, as indicated by the intensity variation on ring (110) on the corresponding SAD pattern in Fig. 2(c). This result is in agreement with the previous XRD analyses. Cross-section observations of the samples R_3, R_1, and R_0 are reproduced in Fig. 3. The samples exhibit a more or less

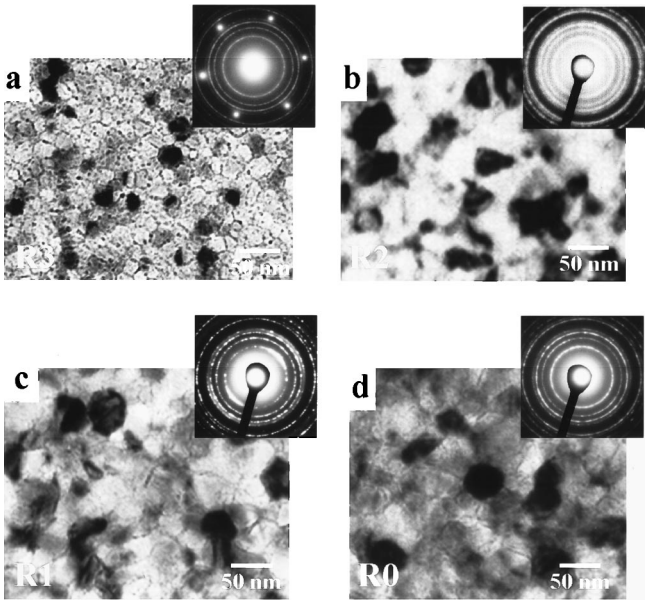

FIG. 2. Plane-view TEM micrographs and their corresponding selected area diffraction patterns obtained, respectively, on (a) sample R_3, (b) sample R_2, (c) sample R_1, and (d) sample R_0.

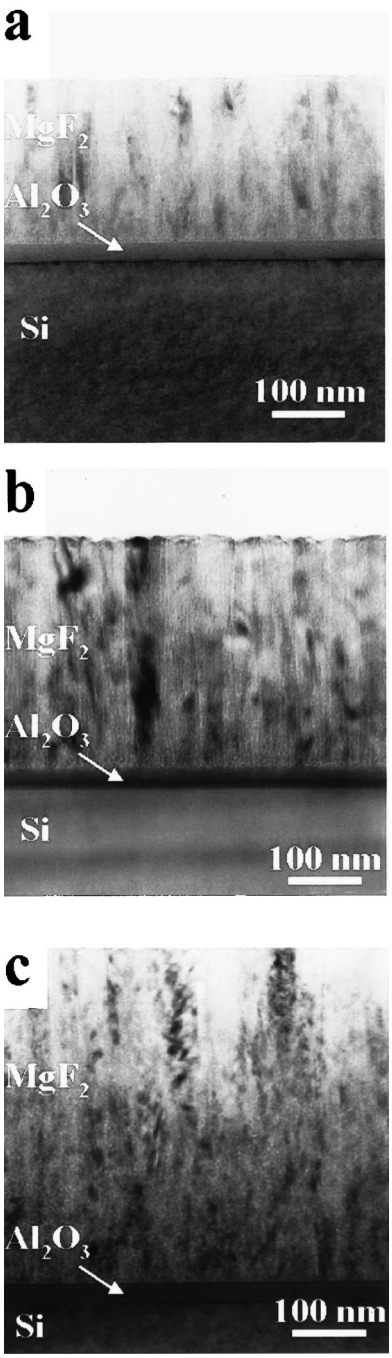

FIG. 3. Cross-sectional TEM micrographs obtained, respectively, on (a) sample R_3, (b) sample R_1, and (c) sample R_0.

well-developed columnar structure and an exceptional compactness. Sample R_3 exhibits a very regular structure. Sample R_1 tends to have conic columns. For the R_0 sample, the microstructure appears less regular: close to the alumina interface, it consists of small grains (globular growth mode) and it evolves to a columnar strongly *V*-shaped growth mode as the thickness of the layer increases. Finally, we also note increasing surface roughness from sample R_3 to R_0.

The chemical composition of each sample has been analyzed. As a typical result, Fig. 4 displays the atomic concentration depth profile of elements for the R_3 sample as measured by XPS. The fluorine and magnesium contents are found to be very constant across the whole layer, indicating the very good homogeneity of the coatings and also the reliability of the measurement method. Indeed, any fluorine desorption which could be due to the Ar^+ bombardment used for the analysis has not occurred during the measurement. Furthermore, Mg and F ratio is in good agreement with the MgF_2 bulk stoichiometry. Finally, the very low level of oxygen confirms the lack of water in the films. The other samples exhibit the same kind of composition depth profiles. In Table II, the average atomic concentrations of the films are summarized for all the samples, including also data on contaminant levels. As not expected, these results indicate that, whatever the sample and deposition conditions, all the coatings exhibit a very good stoichiometry, within the experimental error ($F/Mg = 2.00 \pm 0.05$). Moreover, very low levels of contamination in carbon and oxygen are measured in the layers, generally lower than 2% and 1%, respectively. We note, in particular, that sample R_3 exhibits slightly higher C and O concentration levels, due to a higher initial base pressure ($\sim 10^{-7}$ mbar) before deposition.

Finally, the optical properties of the samples have been investigated. We focused our work on the extinction coefficient dispersion curves as presented in Fig. 5. Contrary to the compositional results, a very pronounced change in the optical properties is observed from one sample to another. From R_0 to R_4, the absorption clearly decreases especially in the DUV part of the spectral region. Moreover, the absorbing coatings exhibit a characteristic absorption peak located at $\lambda = 260$ nm. This feature is typical of color centers as frequently reported in literature for MgF_2 crystals.[10] In order to check the stability of the absorption observed on the different layers, some of them have been submitted to annealings.

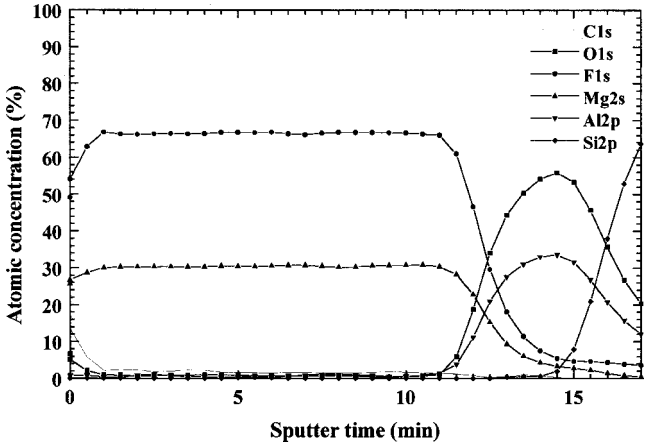

FIG. 4. Atomic concentration depth profiles of the sample R_3 as measured by XPS.

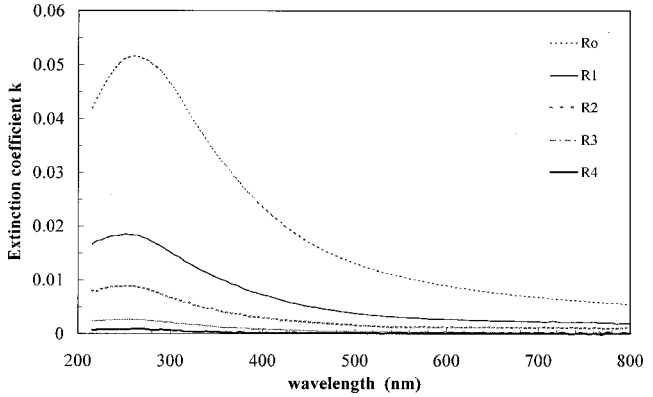

FIG. 5. *K* spectra of as-deposited samples deduced from spectrophotometric measurements.

Both UV and thermal annealings have been performed. Figure 6 describes the evolution of the *k* spectrum of the R_0 sample after a first UV annealing during 2 h under a Hg lamp followed by different thermal annealings at different temperatures. After the first UV treatment, the main absorption peak tends to split into two different absorption peaks approximately centered at 225 and 300 nm. Then, subsequent thermal annealings promote the increase of the 300 nm centered peak at the expense of the 225 nm centered peak. Nevertheless, in the DUV spectral part, the overall absorption remains very high, even after annealings up to 350 °C. Decreasing the absorption significantly requires temperatures as high as 400 °C. On the contrary, the behavior of the other samples deposited in reactive deposition conditions is very different. As illustrated by sample R_2 (Fig. 7), whatever the annealing mode, thermally or UV activated, a drastic decrease of the absorption is observed. The low temperature thermal treatment ($T=100$ °C) makes the absorption decrease but its effect saturates. A subsequent short UV annealing has, however, a strong effect leading to the complete drop of the absorption band. That means that samples deposited in reactive conditions are easily curable.

IV. DISCUSSION

The first noticeable result of this study is that the properties of the films drastically change with the deposition conditions. This is particularly true for the mechanical and optical properties. Though this result is not surprising, this is, however, not the case as far as the chemical composition is concerned. There is, apparently, a contradiction between the strong evolution of the *k*-dispersion curves from one sample to another and the unchanged stoichiometry of the films. Moreover, the fact that all the films exhibit a good stoichiometry with F/Mg equal to 2 is quite unusual, since most of the investigations made by different authors on fluorides deposited by sputtering, state that the fluorine to metal ratio is lower than the ideal one with an absolute decrease of the ratio frequently in the range of -0.1 to -0.5. For instance, in a previous study we made on IBS YF_3[4] we found, under nonreactive deposition conditions, a F/Y ratio of 2.3 instead of 3. The same trend was observed by other authors on IBS MgF_2 coatings since they measured F to Mg ratio as low as 1.6.[6] Finally, on MgF_2 films deposited by cathodic sputtering,[5] Martinu, Biedermann, and Holland reported F/Mg in the range of only 1, or even less.

It is then necessary to check our results by closely analyzing the experimental data, in particular the $k(\lambda)$ spectra. The specific shape of the $k(\lambda)$ curves suggests the presence of color centers in the films, which means fluorine vacancies, each one being occupied by one or more electrons. In the past, extensive research activities were focused on the creation of color centers in MgF_2 crystals.[10–12] From this work, we know that many kinds of color centers can be generated

TABLE II. Average layer atomic concentrations (in percentage) of C, O, F, and Mg in the layer as measured by XPS for all the samples.

	R_0	R_1	R_2	R_3	R_4
C (%)	1.4	1.4	1.2	1.7	1.4
O (%)	0.7	0.4	0.3	0.8	0.4
F (%)	64.3	64.6	65.0	64.2	65.0
Mg (%)	32.1	32.5	32.1	31.9	32.3
F/Mg	2.0	2.0	2.0	2.0	2.0

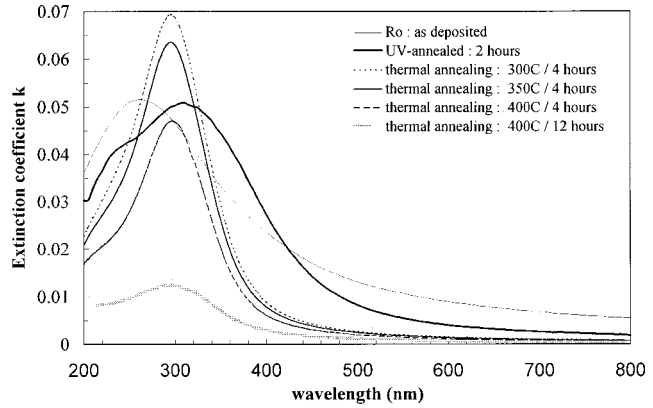

FIG. 6. *K*-spectrum evolution of the *nonreactively* deposited sample R_0 after various post-treatments.

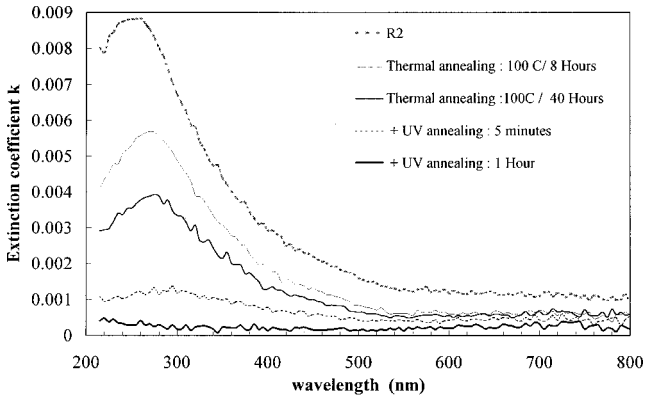

FIG. 7. *K*-spectrum evolution of a *reactively* deposited sample after various post-treatments: example of sample R_2.

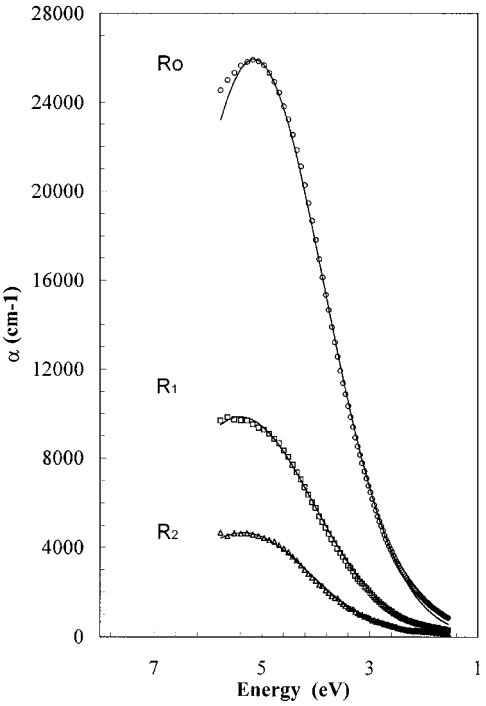

FIG. 8. Experimental absorption spectra and corresponding Gaussian fitting curves (solid line) for three different samples.

in MgF_2 crystals, the most frequent ones being the F center which induces an absorption peak centered at $\lambda = 250-260$ nm and the M center located at $\lambda = 370$ nm. In order to clearly elucidate the kind of centers which are responsible for the absorption we found in our film, we have tried to fit our experimental curves using the model developed, for instance, by Dexter.[13] According to this model, it is possible to calculate the color center concentration from the $\alpha(E)$ curve, where α is the absorption coefficient related to the extinction coefficient by the well known relation $\alpha = 4\pi k/\lambda$ and E is the energy $[E(\text{eV}) = 1.24/\lambda(\mu\text{m})]$. If we assume a Gaussian dispersion of $\alpha(E)$, the color center concentration N is given by the Smakula formula

$$N(\text{cm}^{-3}) = 0.87 \times 10^{17}[n/(n^2+2)^2] \cdot f^1 \cdot \alpha_0 \cdot U,$$

where n is the refractive index of the material at the centering wavelength of the absorption peak, f is the oscillator strength of the color center, α_0 is the absorption coefficient at the peak, and U is the half-width of the band. Near the absorption peak and at its maximum, we take n equal to 1.41 and it is usual to assume $f \sim 1$.[14]

In the case of our IBS films, we fitted their absorption spectra $\alpha(E)$ with a Gaussian whose equation is $\alpha(E) = \alpha_0 \text{EXP}[-(E-E_0)^2/W_0^2]$. W_0 is a fit parameter which is related to U by the relation $U = 2(\ln 2)^{1/2} W_0$. The fit has been particularly optimized in the DUV and UV regions of the spectra. Whatever the sample, we found that it was possible to reasonably fit the absorption curve with only one Gaussian which indicates the contribution of only one kind of color center. Figure 8 gives some examples of experiment-theory comparison and Table III indicates the different fit parameters. The agreement between measurement and theory is rather good. We just note, in particular for R_0, a slight discrepancy in the left side of the peak, near 6 eV. This could result from a displacement of the fundamental absorption edge towards lower energies due to disorder in the coating crystallographic structure as often observed in amorphous or small polycrystallized materials. It is known indeed that disorder can induce new electronic states in the electronic band gap, which forms so-called band tails, that way reducing the optical band gap. From Table III, we see that for as-deposited films the absorption peak is centered at an energy between 5.15 and 5.4 eV, which means around $\lambda = 235$ nm. Even if this value is slightly lower than the wavelength of 260 nm generally reported for the F center in MgF_2 crystals, there is no doubt that the absorption of our films is dominated by F-center absorption (one electron trapped on a fluorine site). In fact, as illustrated by Fig. 9, the centering wavelength of the absorption peak is found to shift, after annealing, to higher wavelengths, up to 253 nm (or 4.9 eV). The reason for this shift could be the decrease of the absorption near the band edge ($E > 6$ eV) and the narrowing of the band tails in the energy band gap leading to a reduced distortion of the α (λ) curve. Further optical investigations in the vacuum ultraviolet (VUV) spectral range down to $\lambda = 120$ nm would be required to check this assumption. Furthermore, as indicated in Table III, the half width of the absorption band (U) was found to be in the range 2.5–3.2 eV. Compared to data reported by Sibley and Facey[10] for MgF_2 crystals with values of 0.806 eV at $T = 300$ K, our values are rather high. We have then a broadening of the absorption band related to the polycrystalline nature of our films which, moreover, tends to decrease with the reactive conditions when the film structure is less disordered.

As a consequence of the presence of F centers, there are fluorine vacancies in the films, whose concentration N_V can be calculated using the Smakula's formula. Moreover, if we consider that these fluorine vacancies correspond to fluorine atoms missing in the material, it would normally induce a deviation from stoichiometry $\Delta(\text{F/Mg})$ which can be calculated by the following expression:

$$\Delta(\text{F/Mg}) = -N_V/N_{\text{Mg}},$$

TABLE III. Fit parameters for the absorption curves and deduced concentrations of F-vacancies and F/Mg ratio deviations.

Sample	α_0 (cm^{-1})	W_0 (eV)	E_0 (eV)	U (eV)	N_v ($\times 10^{20}\,cm^{-3}$)	Δ(F/Mg) ($\times 10^{-3}$)
R_0	25 950	1.84	5.15	3	6	−19
R_1	9860	1.92	5.4	3.2	2.4	−8
R_2	4670	1.76	5.35	2.93	1.05	−3
8 H-annealed R_2	2800	1.58	5.05	2.6	0.56	−2
40 H-annealed R_2	1920	1.48	4.9	2.46	0.36	−1
R_3	1370	1.73	5.27	2.88	0.30	−1
R_4	450	1.48	5.2	2.46	0.085	−0.3

where N_V and N_{Mg} are the concentration of F vacancies and Mg atoms, respectively. We have $N_{Mg}(cm^{-3})=\rho\mathcal{N}a/M$, with ρ being the mass density (3, 17 g cm^{-3}), $\mathcal{N}_a$ Avogadro number, and M the molar mass of MgF_2. The results are reported in Table III. The data clearly evidence that the concentration of fluorine vacancies is low enough not to noticeably affect the F to Mg ratio since Δ(F/Mg) remains lower than 0.02. This value is far lower than the experimental error of ± 0.05 achieved by XPS, which means that such fluorine deficiency is not detectable by XPS. We can conclude that the experimental composition results are not in contradiction with the optical measurements.

The second noticeable result of this study concerns the typical behavior of the coatings after thermal or UV treatments. Two opposite behaviors have been found which can be summed up as follows: (i) a nonreversible optical absorption for the IBS films when deposited in nonreactive deposition conditions; (ii) an easily curable absorption for samples deposited in reactive conditions. Moreover, in this second case, the temperature needed for a modification of the absorption is particularly low: 100 °C corresponding to an energy of 0.03 eV. Catlow, James, and Norgett[15] have reported on the energies of activation for different diffusion mechanisms in MgF_2 crystals. Their calculations state that the rutile crystallographic structure of MgF_2, as a noncompact structure, offers diffusion paths which require low energy of activation. Thus, as far as fluorine vacancies are concerned, among the different available transitions, the easiest diffusion mechanism corresponds to the transition path denoted w_3 (as illustrated on Fig. 10) which requires an energy of activation of only 0.03 eV. The other mechanisms consume higher energies, 0.31 and 1.53 eV for w_1 and w_2 jumps, respectively. Our results seem then to be consistent with the w_3 low energy mechanism. Nevertheless, since after annealing we observe a clear decrease of the absorption band, that is to say, a decrease of the F-center concentration (see Table III), a recombination mechanism must occur in the material. Such a recombination which results from interactions between an electron, a F vacancy, and a fluorine atom, implies having some free fluorine in the material. This fluorine could come from F atoms positioned in interstitial sites and/or at grain boundaries. During the first low temperature annealings, the recombination at the grain boundaries by step by

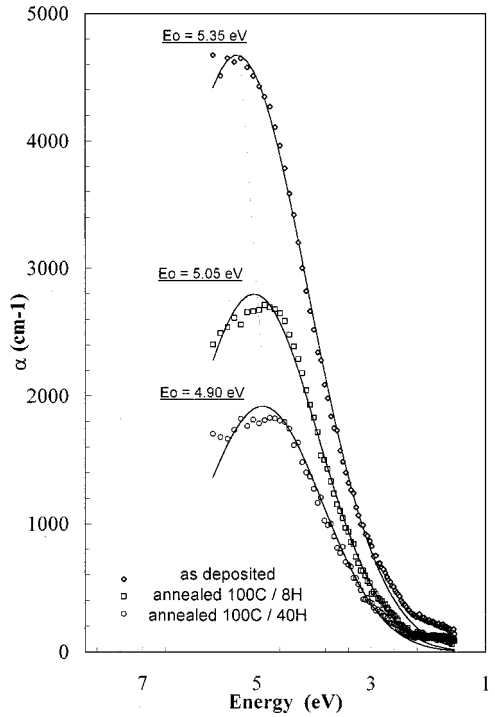

FIG. 9. Evolution of the experimental absorption spectra and their corresponding Gaussian fitting curves (solid line) after various thermal annealings: example of sample R_2.

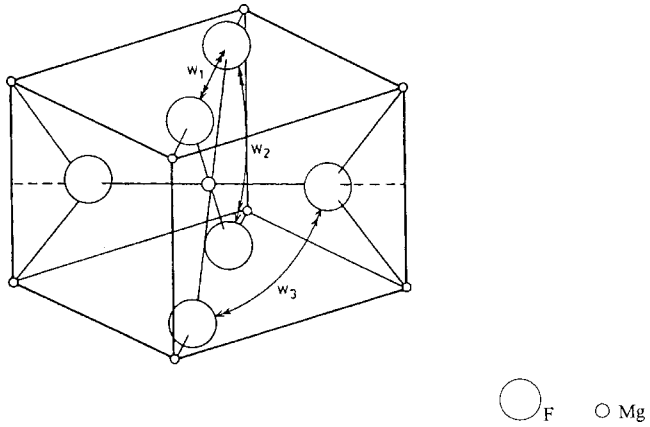

FIG. 10. *F*-vacancies diffusion paths in MgF_2 crystal (from Ref. 15). The *c* axis is vertical and the energies of activation are 0.31 eV (w_1); 1.53 eV (w_2), and 0.03 eV (w_3).

step migration of F vacancies towards the grain surface is probably the dominant mechanism. Such a mechanism would be, indeed, less energy consuming since it does not require supplementary energy for F migration from interstitial to F sites. Nevertheless, the necessity of using UV-activated annealing afterwards to completely bleach the material pleads in favor of a second mechanism as recombinations between F color centers and interstitial F atoms. The Hg-UV lamp exhibits indeed a strong ray emitting at $E \sim 5$ eV, which corresponds to the energy required to suppress an anion-Frenkel-pair defect.[15] Furthermore, the fact that the films deposited under reactive conditions exhibit compressive stresses tends to prove that some supplementary fluorine could lie in the material at wrong positions. The annealing of the films by replacing the F atoms in the right positions would then induce a mechanical relaxation of the coatings, which has not been proved yet.

Concerning now the R_0 sample, the various annealings only affected the shape of the absorption curve. Such a change looks quite similar to the photothermal conversion effects reported by Baryshnikov *et al.*[12] observed on annealed MgF_2 crystals which they had previously made fluorine deficient by electron beam irradiations. Among the different absorption bands which arose in the absorption spectrum after successive annealings, they identified a band at $\lambda = 300$ nm whose origin is unfortunately not clear. Our results are too limited to go deeper into the discussion, but the fact that the R_0 sample keeps its absorption high shows that no color center recombination seems to occur in the material. It means that there is either no free fluorine available or the structural disorder in the layer prevents the diffusion mechanisms from happening at low activation energy. Our TEM analyses have clearly evidenced that our deposition conditions, when reactive, promote a far more regular arrangement of the grains in the coatings. Moreover, a slightly preferential orientation of the grains with their (110) plans parallel to the coating surface is observed. As illustrated in Fig. 10, the activation energy of the F vacancies strongly depends on the crystallographic directions and is much higher along, for instance, the C axis (w_2 path). In a columnar structure where the column height corresponds to the thickness of the coating (200–300 nm) and the column width ranges from 25 to 40 nm, if we assume some recombinations to occur at the grain interface, it is clear that diffusion paths perpendicular to the columns would be more favorable. We suggest here that the preferential orientation of the columns observed in R_1–R_4 samples, by aligning more or less the ''low energy'' w_3 path along the diameter of the columns, may help the recombination mechanisms to happen.

V. CONCLUSION

This study shows that the advanced IBS fluoride process we developed enables the production of very low UV absorbing MgF_2 films which exhibit a bulk-like low refractive index. Contrary to previous works, the fluorine deficiency, even in nonreactive deposition conditions, remains extremely low. Microstructure differences between the samples, depending on the deposition conditions, have been evidenced: the samples deposited in reactive conditions exhibit regular columnar microstructures (slightly ⟨110⟩ textured), whereas the sample deposited in nonreactive conditions exhibits a more irregular and randomly orientated microstructure. Moreover, the results show that the improvement of the optical properties is connected with a change of the mechanical stress in the films from tensile to more and more compressive.

The origin of the residual absorption has been identified as due to F centers in the material. On the basis of a simple color center model, the concentration of these centers has been calculated and found to be very low. Such a result emphasizes the particularly high sensitivity of MgF_2 films to fluorine vacancies, as far as optical absorption is concerned. Moreover, the reactive deposition conditions, by greatly improving the arrangement of the structure of the films, seem to make the optical recovery of the films easier provided that we assume free atomic fluorine to be available. On the contrary, the disturbed structure of films deposited in nonreactive deposition conditions by promoting the high stability of the strong optical absorption could explain the fact that these films are not curable.

ACKNOWLEDGMENTS

The authors gratefully acknowledge the support of the European Commission (TMR-network UV coatings, Contract No. ERBFMRX-CT97-0101). Many thanks are due to J. C. Ferrer for XPS measurements, and X. Alcobé and J. Bassas for XRD measurements. The authors would also like to thank B. Rolland for the film preparation, O. Lartigue for his technical support in spectrophotometry, and A. Petit dit Dariel for useful discussions on color center modeling.

[1] E. Eva, K. Mann, N. Kaiser, B. Anton, R. Henking, D. Ristau, P. Weissbrodt, D. Mademann, L. Raupach, and E. Hacker, Appl. Opt. **35**, 5613 (1996).
[2] J. D. Targove, Ph.D. thesis, University of Arizona, 1987.
[3] M. Kennedy, D. Ristau, and H. S. Niederwald, Thin Solid Films **333**, 191 (1998).
[4] E. Quesnel, M. Berger, J. Cigna, D. Duca, C. Pellé, and F. Pierre, Proc. SPIE **2776**, 366 (1996).
[5] L. Martinu, H. Biedermann, and L. Holland, Vacuum **35**, 531 (1985).
[6] T. H. Allen, J. P. Lehan, and L. C. McInctyre, Jr., Proc. SPIE **1323**, 277 (1990).
[7] H. Schink, J. Kolbe, F. Zimmermann, D. Ristau, and H. Welling, Proc. SPIE **1441**, 327 (1990).
[8] E. Quesnel, J. Dijon, L. Dumas, P. Garrec, C. Pellé, L. Poupinet, and B. Rolland, Proceedings of Optical Interference Coatings, Tucson, AZ, OSA Technical Digest Series 9, 1998, p. 47.
[9] H. Blaschke, R. Thielsch, J. Heber, N. Kaiser, S. Martin, and E. Welsch, Proc. SPIE **3578**, 74 (1998).
[10] W. A. Sibley and O. E. Facey, Phys. Rev. **174**, 1076 (1968).
[11] R. F. Blunt and M. I. Cohen, Phys. Rev. **153**, 1031 (1967).
[12] V. I. Baryshnikov, L. I. Shchepina, S. V. Dorokhov, and T. A. Kolesnikova, Opt. Spectrosc. **73**, 291 (1992).
[13] D. L. Dexter, Phys. Rev. **101**, 48 (1956).
[14] N. Seifert, S. Vijayalakshmi, Q. Yan, A. Barnes, R. Albridge, H. Ye, N. Tolk, and W. Husinsky, Radiat. Eff. Defects Solids **128**, 15 (1994).
[15] C. R. A. Catlow, R. James, and M. J. Norgett, J. Phys. Colloq. **37**, 443 (1976).